MICROSTRUCTURAL CHARACTERISTICS-PROPERTY RELATIONSHIPS IN CAST IRONS

T. Alp[1], F. Yilmaz[2] and A. A. Wazzan[3]

[1:]*Professor, Chemical & Materials Engineering Department, King Abdulaziz University.*
2:Professor, Metallurgical Engineering Department. Sakarya University, Adapazari, Turkey.
3:Assistant. Professor, Chemical & Materials Engineering Department, King Abdulaziz University.
P.O.Box 80204, Jeddah 21589, Saudi Arabia, e-mail: tyalp1@hotmail.com

ABSTRACT

Several cast irons, prepared with different chemical compositions and microstructures have been examined by extensive mechanical testing and optical and scanning electron microscopy (SEM). Properties arising from various microstructures are tabulated. Mechanical properties are shown to be a function of both the martix and graphite (or carbide) forms. Changing the matrix from ferritic-pearlitic to bainitic-martensitic type results in effects similar to those experienced in steels containing these phases respectively. The influence of graphite (or carbides) on the final properties, however, is dictated by the respective shapes and distributions of these microstractural constituents. The coupled zone-eutectic region in gray cast iron is asymmertical and inclined to the right-hand side in Fe-C equilibrium phase diagram. Consequently, hypereutectic compositions reveal denderites of primary austenite. In white cast iron, the coupled zone symmetry is thought to arise from the high volume fraction of cementite which compensates for its growth rate anisotropy.

Keywords: *cast irons, microstructure, mechanical properties, graphite, carbide, coupled zone.*

( )

( )

( )

)   Fe-C

1.   INTRODUCTION

Cast irons have been traditionally named according to either their microstrucrures or the heat treatments which they undergo. Chemical and mechanical properties are rarely used for identification. Constitutional descriptions are often based upon two of the phases present in the microstructure.

Until recently, cast irons have been categorized according to the distribution of their respective graphite phase as typified by the specification ASTM A247. In view of the researches [Loper Jr., et al., 1981, Liu, et al., 1980, Double, Hellawell, 1974] that have shown cast iron structures to be much more complex than thought originally, there is a growing concern to amend the specifications used hitherto in order to take into consideration the newly observed morphologies. In grey cast iron, for instance, a variety of graphite shapes and distributions add to the complexity. The ASTM classification generally relies on the various patterns of graphite distribution as illustrated in Fig.1. Type-D flake morphology in this classification, for example, when examined by optical microscopy, closely resembles coral graphite. However, this doubt is fully resolved by using scanning electron microscopy (SEM). Hence, one of the objectives of the present work has been to redefine graphitic cast irons according to the morphology of their graphite phase, identfy the condition and mechanisms leading to their growth, and elucidate some of the important crystallographic and microstructural features. The second major objective has been to indicate the strong influence exercised by the microstructural state on the mechanical and physical properties. Since these properties are dependent upon graphite shape and distribution, in this work special emphasis is laid upon the shape factor and all graphitic cast irons, including the malleable cast iron, are examined from this perspective. In white cast iron, carbide as a competing phase with graphite, is also investigated. Consequently, in the present paper, graphitic cast irons are classified as flake-lamel, coral-fibrous, vermicular-cylindrite and spheroidal-nodular respectively.

2.   EXPERIMENTAL DETAILS

Cast irons prepared individually by high frequently (HF) electromagnetic field induction melting were first subjected to tensile tests at a crosshead speed of 2 mm per minute, using an Instron universal testing machine model 6025. Additionally, Brinell hardness tests were carried out. Metallographic studies of unetched or lightly/heavily etched samples were conducted by using optical microscopy. Specimen surfaces were deep etched for SEM investigations. Deep etching for 10 hours in 15% HCl acid solution was followed by cleaning for 10 minutes with 5% hydrofluoric acid. The period of deep

etching depends on both the concentration of the etchant and its renewal. The cleaning in hydrofluoric acid was continued until the bubbling action subsided. Although etching and cleaning times are a function of fineness of structure, the matrix was also found to be an important factor. The rate of attack was large for the γ and α matrix. In contrast the pearlite seemed to exhibit little depth in long etching. Samples with their surface graphite and/or carbide extracted were rinsed in methanol to remove any acid residue from the surfaces and then thoroughly dried. It should be pointed out that the graphite and carbide phases, which are normally less affected by acid attack show marked deterioration when exposed to acid media over prolonged periods of etching or cleaning. The chemical compositions, solidification conditions and the mechanical test results of various cast irons investigated in this study are presented in Table 1.

3.   MICROSTRUCTURAL OBSERVATIONS

3.1.   Cast Irons with Graphite

3.1.1 Flake-Lamel Graphite Cast Irons

These irons may be subdivided into various groups according to the liquid composition and solidification conditions (Fig.1). In type-C coarse primary flake graphite crystals are observed at hyper-eutectic compositions. These crystals are a few mm in length and a few hundred μm in width. They can be differentiated from the eutectic flakes by their coarse forms and smooth surfaces. Cooling rate was found to exercise a dramatic effect on the size and distribution of the graphite crystals. Increasing the cooling rate leads to fine graphitization and favours type-A against type-B formation. Type D and E graphites form for all compositions at high cooling rate, and in the case of hypo-eutectic compositions they form irrespective of the cooling rate.
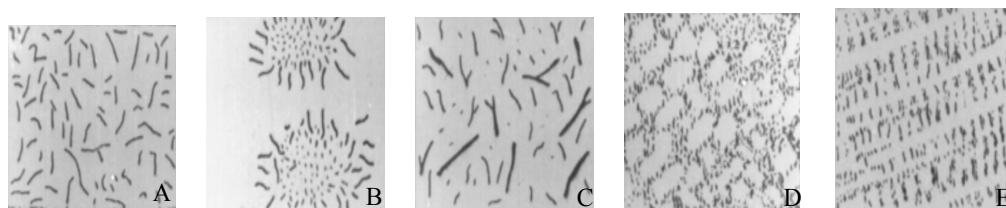
Fig. 1: Types of flake graphite according to ASTM A247.

Fig. 2b indicates flake graphite in three dimensions associated with twist and rotational faults. Graphite has a hexagonal structure the unit cell of which is defined by two (0001) basal planes and six ($10\bar{1}0$) rectangular planes perpendicular to the basal planes (Fig. 3a). Carbon atoms in the basal planes have strong covalent bonding, while adjacent basal planes are held by weak van der Waal forces. The basal planes have the appearance of a

stack of layers in several thicknesses [Double, Hellawell, 1969]. Individual layers are 10^{-5} cm in thickness and show rotations about the C axis of ~ 13° ~22° and 28° (Fig.3c). Flake graphite grows from nuclei formed on twist boundaries. Crystal growth occurs along the basal plane by using these steps. This is referred to as A-growth. In the case of flake crystals there is little growth along the direction perpendicular to the basal plane. This is termed C-growth. Coarsening of flake crystals, changing of orientation, branching and bending provide convincing evidence that C-growth in these crystals is negligibly small.
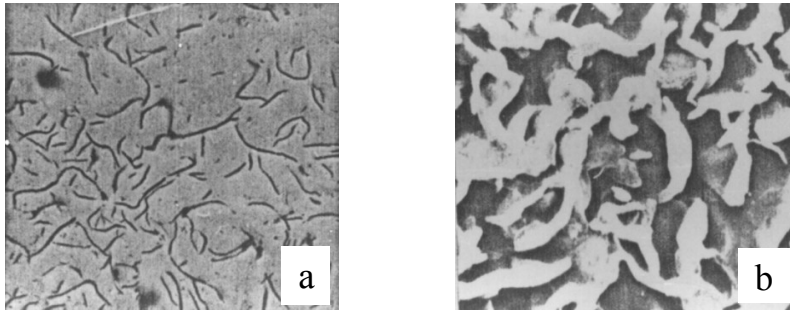
Fig. 2: Flake-lamel graphite cast iron a) Optical micrograph, x110, b) SEM micrograph, x400.
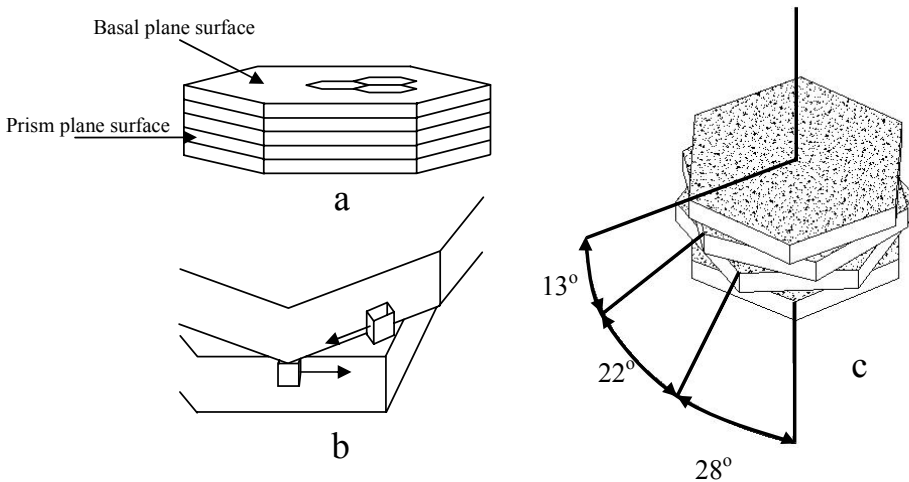
Fig. 3:   Flake graphite. a) Basal and prism planes, b) Growth in a-direction by step of twist
        boundary, c) Rotations of growth layers.

Due to the presence of multiple steps on ($10\bar{1}0$) planes, growth on these surfaces is relatively easier than could progress on faceted (0001) surfaces. The presence of thermal and compositional gradients in front of the growing crystal prevents the stable growth of graphite. Change of orientation, bending and branching, which are seen in lamellar growth, in normal eutectics, are also observed in flake graphite growth. There are two mechanisms that could operate for the branching and bending of flakes. The first of these involves straight orientation change of growing (0001) plane by twinning ［Double, Hellawell, 1969, Nieswaag, Zuithoff, 1974］ and the second is associated with flake branching in growing (0001) plane by the occlusion of foreign particles [Lux, et al., 1974].

3.1.2. Fibrous-Coral Graphite Cast Irons

Increasing the cooling rate leads to a shift from A-type coarse flake to undercooled D-type flake. The undercooled flake, on the other hand, transforms to fibrous graphite with further increase of cooling rate. Flake graphite exhibits a lamellar feature in contrast to fibrous graphite, which manifests a circular section and rod like character. In these crystals there is no abrupt corner so that growth continues uninterruptedly. Figure 4 illustrates observation of fibrous graphite. The SEM evidence shows rounded growth feature as well as weak lamellar in fibrous crystals.
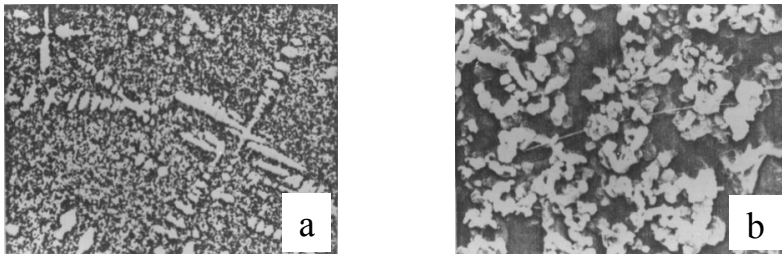
Fig. 4: Fibrous coral graphite cast iron, a) optical micrograph x150, b) SEM micrograph x1200.

[Lux, et al., 1974] have convincingly shown that the crystal either grows along C-direction perpendicular to the (0001) planes as sketched in Fig. 5b, or along a-direction by scrolled or conical development of (0001) planes (Fig.5 a, c). The growth of graphite along c-direction requires two dimensional nucleation or screw dislocation sites; but even then this type of growth is unfavourable. Relatively easy growth occurs when basal planes lie parallel (scroll) or semi-parallel (conical) to the axes of fibres.
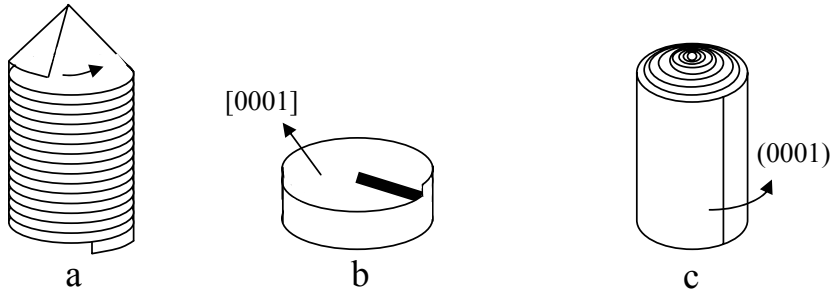
Fig. 5: Fibrous graphite growth models based on [Lux, et al., 1974] data, a) Conical forms,
b) Growth by screw dislocation c) Scrolled form.

3.1.3 Cylindrical -Vermicular (CV) Graphite Cast Irons

This type of graphite growth is observed in alloys containing insufficient spheroidiser (0.02% Mg). Inter-connected cylindrical growth is evident in Fig. 6. This crystal form lies in between degenerate flake-fibrous and spheroidal growth forms. While spheroidal graphite shows separate nucleation and growth, cylindrical graphite exhibits conjoint nucleation and continuous growth. Excessive Mg addition (0.05%Mg) leads to transformation from cylindrite to nodular form.
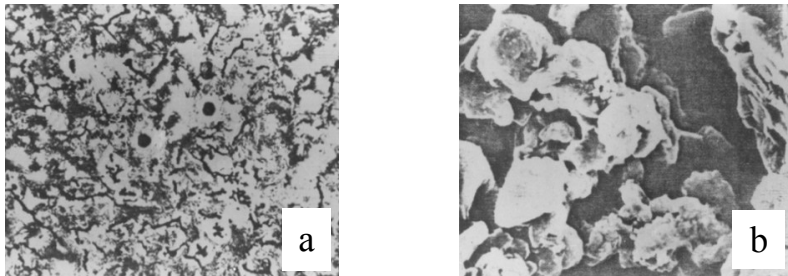
Fig. 6: Cylinderite vermicular graphite cast iron, a) Optical micrograph x110.
b) SEM micrograph x1600.

3.1.4. Nodular-Spheroidal Graphite Cast Irons

Using differential thermal analysis (DTA) it has been shown [Lacaze, et al., 1997] that cooling rate in the range 1-20 K/min., affects the onset of the ferrite growth in spheroidal graphite (SG) iron. The temperature for the start of this transformation in a base Fe-C-Si alloy is decreased by small addition of Mn or Cu.

SG growth occurs from individual and separate nuclei present in the liquid. It is suggested that spheroidal graphite develops as a result of two dimensional growth on (0001) planes. This type of growth in the c-direction can be aided by screw dislocations. An alternative suggestion involves growth in the [10$\bar{1}$0] direction of wrapped (0001) planes. These planes develop in a continuous manner by giving rise to tilt-twist boundaries. Deep etching of polished surfaces has consistently revealed tilt-twist boundaries. However, extension is always along the a-direction. As the (0001) planes continue to warp, the overall growth of the nodule occurs in the [0001] direction. This "cabbage-like" growth, which is frequently observed on the surface of graphite crystals, is illustrated in Fig. 7.

SG sections are observed to embody conical segments when examined by optical microscopy (Fig. 8a). This depicts a good example of symmetrical growth which involves tilt-twist boundary. As seen in Fig. 8b, the traces in the segment are reminiscent of helical growth. Cylindrical graphites may grow either in a helical or wrapped manner (Fig. 8b and 8c). Optical and SEM evidence presented in Fig. 6 supports this suggestion. In the optical micrograph three different features are noteworthy. These are the cylindrical structure, star-like structure and spheroidal structure. The star-like structure, which is covered by a-halo, is not related to the growth model of Fig. 8d. This structure develops under active nucleation condition. Following nucleation, this crystal showed rapid initial growth until actual obstruction by Mg occurred. Initial growth was edgewise in the a-direction which led to thickening. Two-stage growth as presented here for the Fe-C system has also been reported for the Al-Ge [Lemaignan, et al., 1981] and Al-Si [Yilmaz, 1979].
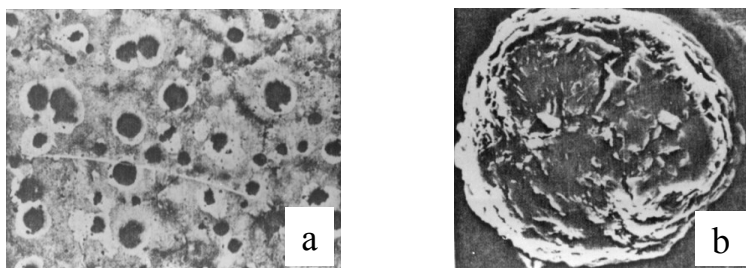
Fig. 7: Nodular-spheroidal graphite cast iron, a) Optical micrograph x100,
b) Extracted graphite (SEM x1600)
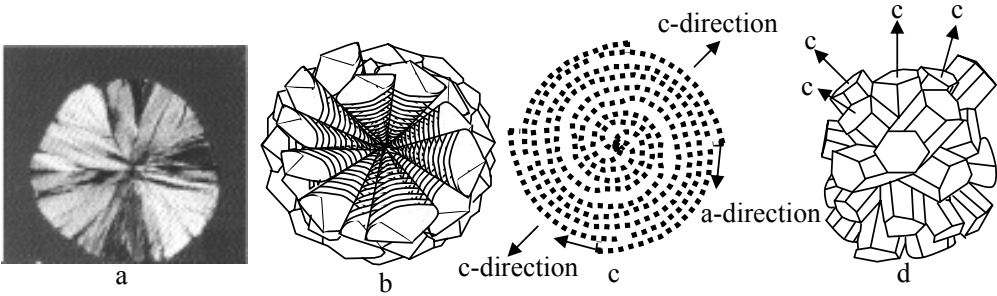
Fig 8: SG growth models, a) Optical micrograph of nodule x800, b) The nucleus of a spherulite,
    c) Cabbage-like growth, d) Star-like branching.

3.1.5. *Temper Graphite Cast Irons*

White irons are heat treated to decompose the metastable Fe_3C into graphite. The final
structure consists of graphite temper rosettes in a ferritic or pearlitic matrix. The
development of temper graphite depends on solid-state diffusion and is influenced by the
carbide structure, composition, tempering temperature and time, as well as the furnace
atmosphere. The microstructure of malleable cast iron is depicted in Fig. 9.
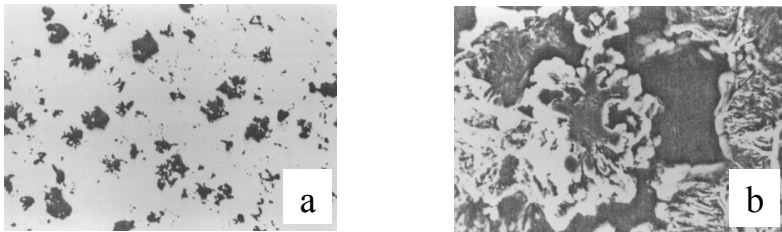
Fig. 9: Temper graphite cast iron a) Optical micrograph x110, b) SEM micrograph x900.

3.2.   Cast Irons with Carbide

Carbides in cast irons may have the general formulae M_3C, or M_7C_3. These carbides may
occur as lamel, rod, or continuous matrix. In unalloyed cast iron, Fe_3C either develops in
a lamellar manner or forms a continuous phase. Any graphite present in the structure
leads to mottled appearance. The carbide phases impart hardness wear and abrasion
resistance. The microstructure of the unalloyed iron generally consists of M_3C carbides
and pearlite as shown in Fig. 10. However Ni, Cr and Co additions both increase the
hardness and toughness. Especially M_7C_3 carbides in these alloys show broken lamellar
structure and display greater toughness. The M_7C_3 carbides are also reported to grow as
rods and blades with their long axes parallel to the heat flow direction in the mould
[Dogan, et al., 1997].
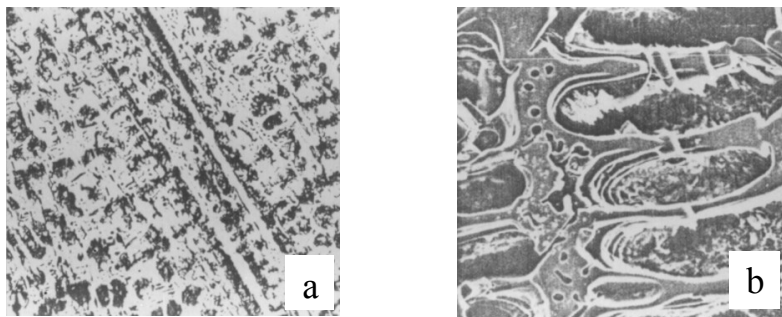
Fig. 10: Cast-iron with carbides a) Optical microstructure x110, b) SEM micrograph x 510.

3.3. Eutectic Growth

In cast irons primary γ grows with non-faceted dendritic morphology. Whilst, primary graphite or carbide grows with faceted lamellar morphology. Primary phases in this alloy are surrounded by a eutectic phase. The eutectic growth region is a zone of composition and temperature. The more rapidly developing phase (γ or graphite) dominates the eutectic structure. The purely eutectic structure extends on either or both side of the eutectic point. The eutectic region develops without primaries. Especially high liquid temperature gradients expand this zone causing coupled eutectic growth to develop easily. The formation of completely eutectic structures has a special significance in relation to certain mechanical properties. When a eutectic structure is produced with controlled orientation composite-like properties are obtained to advantage.

In gray cast iron, the eutectic region extends to the right hand side, while in (WCI) the eutectic region is highly symmetrical [Elliott, 1983, Frediksson, 1975]. Asymmetrical eutectic zone in graphite containing irons is due to the anisotropic growth behaviour of graphite. The near-symmetrical coupled zone in (WCI), on the other hand, is due to high volume fraction of carbide (Fig. 11).
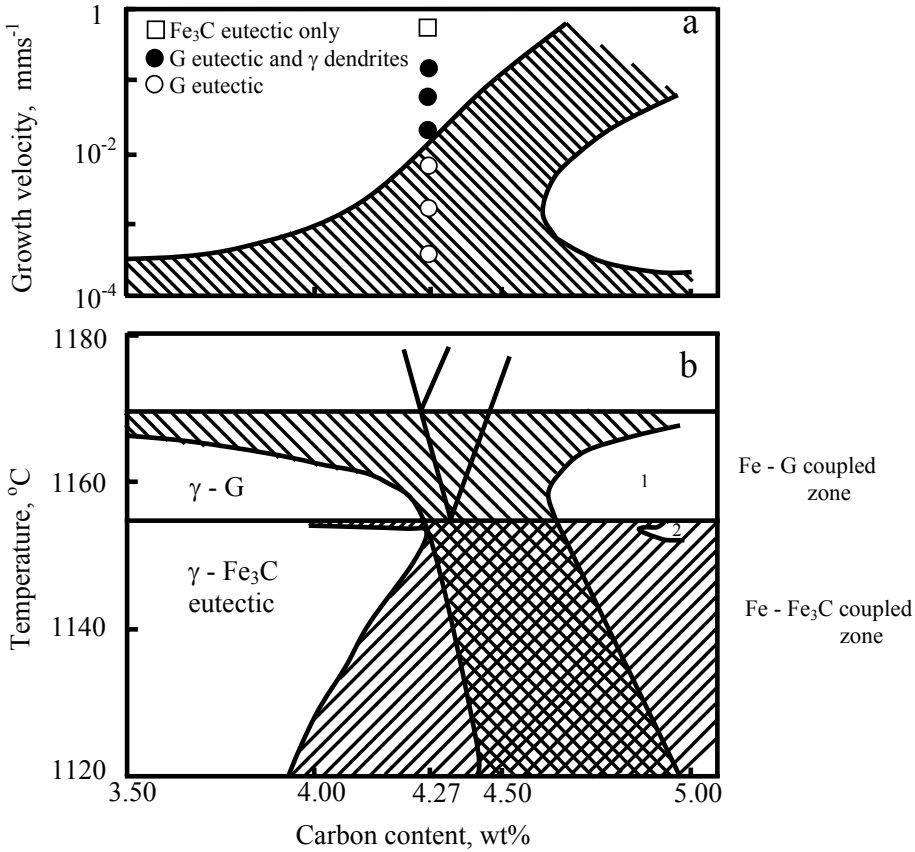
Fig. 11: The coupled zones in directionally solidified Fe-C alloys with G:70 ^{o}C cm^{-1}.

a) Velocity-composition plot showing calculated boundaries and experimental points,

b) Temperature-composition plot with superimposed phase diagram

Region 1. G plates and G eutectic. Region 2. Fe$_3$C plates and eutectic [Dogan, et.al, 1997].

In the case of the spheroidal graphite eutectic, each crystal of graphite is taken to be a eutectic particle. This eutectic forms by separate nucleation and growth of graphite. Star-like crystals nucleate freely and grow by branching and behave as origins of eutectic cells. Each spheroidal form is to be regarded as an unbranched star-like crystal. In vermicular-graphite eutectic, the amount of cylindrite graphite cells cannot be calculated, because the cell boundary is not clearly defined. Eutectic graphites are strongly interconnected. Therefore, the number of eutectic cells appears to be less than that of spheroidal eutectic. In fibrous eutectic, graphite and austenite crystals grow in a coupled manner and the eutectic cell number density changes according to the solidification variables. In the case of flake graphite, the eutectic is like a fibrous one and shows

cooperative growth in the eutectic cell. All the graphite in the unit cell is interconnected. Directional solidification conditions lead to only one eutectic cell with elongated fibrous or flake-like growth. Eutectic growth in (WCI) presents similar complication. However, in the ledeburitic transformation it is much reminiscent of a pearlitic transformation in steel [Hillert and Steinhauser, 1960].

Extensive directional solidification experiments carried out showed that in γ-Graphite eutectic, flake graphites do not develop at right angle to the solid-liquid interface. At a given growth rate, due to equal inter-lamellar distance, there is multiple branching in graphite. Branching compensates for compositional and thermal fluctuations. While carbon enrichment in front of the eutectic austenite occurs, the boundary of γ and graphite is relatively devoid of carbon. The high level carbon concentration in the center of austenite leads either to nucleation of graphite or its branching from the boundary. The graphite developed at austenite pockets provides a typical example for undercooling graphite. For high G/V rates (G being the liquid temperature gradient in front of the solid, and V the growth velocity of the solid interface) the interface is stable and the γ-liquid and the graphite-liquid interfaces share the same line. In this case, branching is less than lamellar development. At intermediate G/V values the graphite-liquid interface leads the austenite-liquid interface and frequent branching at non-stable solid-liquid interface is readily observed. At low G/V values, the γ-liquid interface leads eventually as obstruction of graphite growth becomes preponderant. Then, severe branching and transformation of graphite into fibrous forms is possible. This development can be explained by a competitive growth mechanism (Fig. 12). Thus, at a given undercooling, ΔT_1, flake graphite grows faster than austenite. In this way, while flake graphite leads, austenite
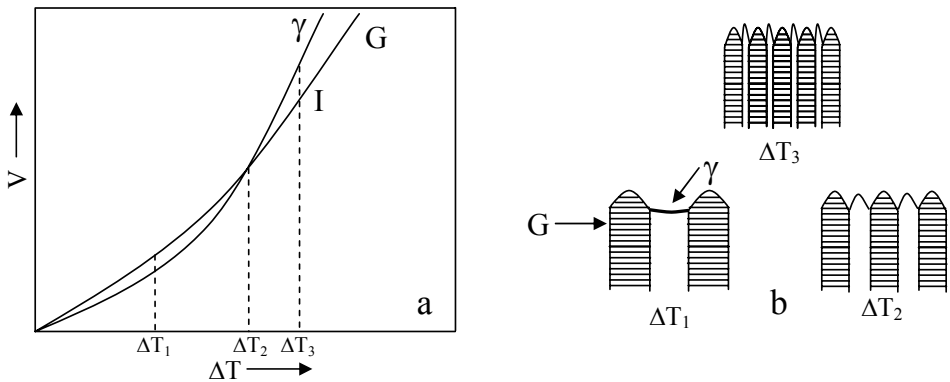
Fig. 12: γ-G. growth in positive temperature gradient a) Growth rate (V) dependence on undercooling (ΔT) for γ and graphite. I represents flake- fibre transition, b) Solid- liquid surfaces.

shows pocket formation in the center. At ΔT_2 (high undercooling) the alternative phases develop with the same growth velocity. At ΔT_3, austenite grows faster than flakes whose growth is frequently interrupted. Consequently, under conditions of progressively higher undercooling (i.e. lower G/V ratios and chill casting) flake graphite transforms to fibrous form.

4.   STRUCTURE-PROPERTY RELATIONSHIP

The solidification of cast iron with a hypoeutectic composition begins with the nucleation and growth of austenite on the mould wall. As the temperature falls, eutectic solidification commences in the interdendritic liquid. This eutectic is either Fe-Fe_3C or Fe-graphite. The proeutectic dendrites strengthen the iron and can be compared to the fibers of a composite. Their strengthening effect depends on their composition, structure, continuity, and fineness. The latter features are promoted by solidification conditions unfavorable to nucleation, namely, high superheat, high pouring temperature, directional growth with a high temperature gradient, low growth velocity, and low solute content. The properties of the dendrites are influenced considerably by the solid-state transformation, which in turn, depends on austenite composition and cooling rate. Pearlite formation which increases the strength of the alloy (Fig.13) is favoured by fast cooling
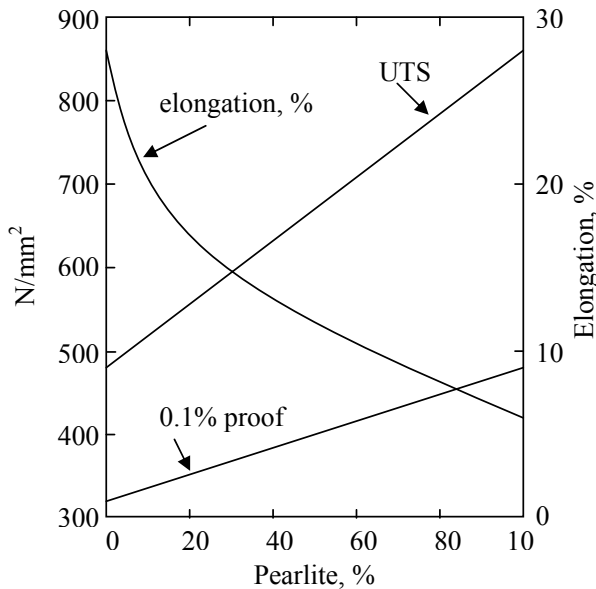
Fig.13: Effect of pearlite fraction on mechanical properties in spheroidal graphite irons [Hillert and Steinhauser, 1960].

rate, low CEV and alloying elements, such as Mn, Ni and Cr and trace elements like Cu, Sn, Sb and As. Heat treatments, such as, austempering in nodular irons, or isothermal heat treatment to produce a bainitic matrix can lead to exceptionally high strengths coupled with good elongation [Cox, 1980].

Table 1 illustrates the fact that in various cast irons mechanical properties are more dependent on microstructure than chemical composition. For example, coarse flake graphite irons (C-type) show lower ultimate tensile strength (UTS) than fine flake graphite irons (A-type). In SG iron, changing the matrix from ferritic structure to pearlitic increases the strength, but decreases ductility. The beneficial effect of stepped austempering on the fracture toughness of SG iron has been interpreted in terms of upper-ausferrite morphology. More intensely interwoven and less sharp needles of ferrite are

Table 1. The structure and properties of various types of cast irons.

No	Type of Cast Iron	Chemical Composition Weight %						Solidification Condition	Mechanical Properties			
		C	Si	Mn	S	P	Others		$\sigma_{0.2}$, MPa	σ_{max}, MPa	$\varepsilon\%$	BHN
1.	Flake graphite	3.31	2.48	0.54	0.037	0.019	Ni(1.25) Mo(1.07)			298		220
2.	Flake graphite	2.95	2.45	0.45	0.033	0.140				365		238
3.	Fibrous graphite	3.81	2.60	0.01	0.002	0.012			334	462	3.5	
4.	Cylindrical graphite	3.5	2.30	0.40	0.010	0.020	Ti(0.08)	Mg(0.02) 44mm,dia.		400	3.0	
5.	Spheroidal graphite (Ferritic)	3.60	2.20	0.40	0.010	0.010		Mg(0.05) 150mm,dia.		400	6.0	
6.	Spheroidal graphite (Pearlitic)	3.60	2.20	0.40	0.010	0.010		Mg(0.05) 44mm,dia.		680	6.0	
7.	Austenitic flake graphite	2.45	1.83	1.02	0.025	0.018	Ni(19.6) Cr(2.16)			210		131
8.	White iron	2.23	0.49	0.43	0.031	0.022	Cr(0.93)					120
9.	Malleable iron (Ferritic)	2.40	1.40	0.50	0.040					340	14	
10.	Malleable iron (Martensitic)	2.4	1.40	0.50	0.180	0.040		Quenched		690	5.0	

$\sigma_{0.2}$ = 0.2% offset yield strength $\varepsilon\%$ = Percent elongation

σ_{max} = Tensile strength   BHN = Brinell Hardness Number

believed to reduce the stress-concentration effect [Hsu and Chuang, 2001]. It is well established that cylindrical-vermicular graphite cast iron shows a thermal conductivity higher than that of spheroidal graphite but less than that of fibrous graphite, in which a highly intimate interconnection between graphite crystals exists. This contributes greatly to conductivity. Spheroidal graphites show no such interconnection, while in vermicular graphites a reasonable degree of connectivity between graphite crystals is observed. An analogous argument will hold when comparing mechanical properties. In fibrous graphite cast iron, due to the good connection between graphite crystals and fine homogeneous distribution, the ductility is 10 times higher than that of flake graphite cast iron.

5.   CONCLUSIONS

1.   In cast irons the nucleation and growth of graphite with novel morphologies is influenced by the degree of undercooling, crystallographic characteristics and alloying additions.

2.   Graphite morphology exercises a strong influence on the mechanical and physical properties of cast irons.

3.   In view of novel new microstractural data pertaining to various morphologies of the graphite phase, new specifications need to be expounded to modify the existing ASTM specifications.

REFERENCES

1.   Cox, G.J., 1980, "The Heat Treatment of SG Iron," *The Metallurgist and Material Technologist*, 12, pp 629-632.

2.   Dogan, O.N., Hawk, J.A. and Laird, H. G., 1997, "Solidification Structure and Abrasion Resistance of High Chromium Wiehte Irons," *Metallurgical & Materials Transaction A.* 28, pp 1315-1328.

3.   Double, D.D. and Hellawell, A., 1969, "The Structure of Flake Graphite in Ni-C Eutectic Alloy," *Acta Metallurgica*, 17, pp 1083-1083.

4.   Double, D.D. and Hellawell, A., 1974, "Growth Structures of Various Forms of Graphite", *The Metallurgy of Cast Iron*," Geneva, pp 509-528.

5.   Elliott, R., 1983, Eutectic Solidification Processing, Butterworths, London, England.

6.   Frediksson H., 1975, "The Coupled Zone in Gray Cast Iron," *Metallurgical Transaction A*, 6, pp 1958-1960.

7.   Hillert, M. and Steinhauser, H., 1960, "The Structure of White Cast Iron," *Jemont Ann*, 144, pp 520-559.

8.   Hsu, C. H., and Chuang, T. L., 2001, "Influence of Stepped Austempering Process on the Fracture Toughness of Austempered Ductile Iron", *Metallurgical and Materials Transactions*, 32A, pp 2509-2514.

9.   Lacaze, J., Boudot, A., Gerval, V., Oquab, D. and Santos, H., 1997, "The Role of Mn and Cu in the Eutectoid Transformation of Spheroidal Graphite Cast Iron," *Metallurgical & Materials Transaction* 28A, pp 2015-2025.

10. Lemaignan, C., Camel, D. and Pelissier, J., 1981, "In-Situ Electron Microscopy of some Solidification Processes in Metallic Alloys," *Journal of Crystal Growth*, 52, pp 67-75.

11. Liu, P.C., Loper Jr., C.R., Kimura, T. and Park, H.K., 1980, "Observations on the Graphite Morphology in Cast Iron," *AFS Transactions*, 88, pp 97-188.

12. Loper Jr., C.R., Voigt, R.C., Yang, J.R. and Sun, G.X., 1981, "Electron Microscope in Studying Growth Mechanisms in Cast Irons," *AFS Transactions*, 172, pp 529-542.

13. Lux, B., Minkoff, I., Mollord, F. and Thury, E., 1974, "Branching of Graphite Crystals Growing from a Metallic Solution," *The Metallurgy of Cast Iron*, Geneva, pp 494-508.

14. Nieswaag, H. and Zuithoff, A.J., 1974, "The Effect of S, P, Si and Al on the Morphology and Growth Structure of Directionally Solidified Cast Iron," *The Metallurgy of Cast Iron*, Geneva, pp 327-351.

15. Yilmaz, F., 1979, Ph.D. Thesis, University of Manchester, Manchester, England.